Chennai extreme rainfall event of 2015 under future climate projections using the pseudo global warming dynamic downscaling method

P. Jyoteeshkumar, P. V. Kiran and C. Balaji*

Department of Mechanical Engineering, Indian Institute of Technology Madras, Chennai 600 036, India

Here we report results of a detailed numerical study on the effect of climate change on the characteristics of a very severe rainfall event that occurred in the coastal city of Chennai, Tamil Nadu, India in December 2015. The pseudo global warming (PGW) method was used to obtain the initial and boundary conditions of the future climate and projections were done for the far future, i.e. the year 2075 using the representative concentration pathway scenario of 8.5. The Weather Research and Forecasting (WRF) model was used for simulations with perturbed initial and boundary conditions by the PGW method in a dynamic downscaling framework. The sensitivities of Microphysics and cumulus parameterization schemes in WRF were first studied. The warm rain microphysics (Kessler) scheme and Kain–Fritsch (KF) cumulus scheme showed good agreement with the observed data. Once the best schemes were identified for such an extreme event and for the specific region under consideration, simulations were carried out for future and current climate conditions. Results show that the bulk Richardson number, energy helicity index, *K*-index, moisture convergence, vertical temperature and mixing ratio all increase significantly in future climate conditions, thereby leading to heavy precipitation. The precipitation in Chennai region increased by 17.37% on the peak rainy day (1 December 2015) in future compared to current. The key takeaway though is that on succeeding days, the amount of precipitation was seen to increase dramatically by 183.5%, 233.9% and 70.8%. This is bound to lead to severe flood events that are likely to continue for more days in the future, thereby posing further risk and potential for damage.

Keywords: Climate change, extreme rainfall events, pseudo global warming method, weather research and forecasting.

INDIA is one of the most vulnerable countries in the world to extreme weather events like tropical cyclones, heat waves and intense rainfall. Annual average fatalities in India due to climate hazards are about 3660, which is the second highest in the world, and the average loss per year is US$ 12,822.708 million (in purchasing power parity)[1]. Floods caused by heavy rainfall are one of the most common natural disasters in India, leading to mass destruction of property as well as a large number of human casualties. During the period 1953–2011, around 1 lakh human lives have been lost in the floods caused by heavy rainfall[2]. The frequency and intensity of extreme rainfall events in India have shown an increasing trend in recent decades[3–5]. According to Mukherjee *et al.*[3], in the past few decades, the increase in rainfall is prominent in the southern part compared to the northern part of the country. The southwest monsoon (SWM) and northeast monsoon (NEM) are the two significant contributors of rainfall in India; NEM contributes around 10–20% of annual rainfall in the country. The southern peninsular India, mainly the Tamil Nadu (TN) coast receives about 50% of its annual rainfall from NEM[6]. Lately, the south Indian states have encountered an increased number of heavy rainfall events leading to massive floods. Kerala, the southwestern state of India, experienced massive floods in two consecutive years, 2018 and 2019. In 2018, Kerala had a record high precipitation in August, leading to massive floods, mainly in the central parts of the state. The massive floods had caused more than US$ 3 billion economic loss and led to the death of more than 400 people[7,8]. In 2019 during the same period, Kerala was again hit by heavy rainfall and associated floods, which led to the death of 125 people[9]. Another major flood that happened in recent years was during 2015 in TN and the Union Territory Puducherry. Chennai city was the most affected region during the flood. The city received 276 mm of rainfall on 1 December 2015 alone, constituting about 76% of the expected seasonal rainfall[10]. Due to this massive flood, more than 500 people lost their lives, and around 1.8 million people got displaced[11]. Changes in atmospheric conditions in a warming world are speculated to be one of the reasons for the increased number of heavy rainfall events in South India.

Many studies have reported that the increase in atmospheric temperature, sea surface temperature (SST) and atmospheric moisture content is due to climate change around different parts of the world[12–14]. According to the 2014 report of IPCC[12], without any mitigation, warming is likely to exceed 2°C, which is the pathway ranging

*For correspondence. (e-mail: balaji@iitm.ac.in)

between representative concentration pathways (RCP) 6.0 and 8.5. According to the Clausius–Clapeyron equation, the increase in atmospheric temperature, increases the moisture-holding capacity of the atmosphere, which leads to an increase in the amount of precipitation. In compliance with earlier studies[15,16], daily precipitation was found to increase by 7% for each degree rise in temperature. Prakash *et al.*[6] showed that increased temperatures and frequent land falling of cyclones aggregate to enhanced NEM rainfall over peninsular India.

In 2015, the increased amount of NEM badly hit the coasts of TN, especially Chennai and Puducherry. The strong upper-level divergence and high moisture content at the lower level were favourable for occurrence of the heavy rainfall event in TN[17]. The strong wind shear together with dry-air advection facilitates favourable condition for heavy precipitation in the state[18]. Boyaj *et al.*[10] used the Weather Research and Forecasting (WRF) model to simulate the 2015 Chennai extreme rainfall event and found that NEM was positively correlated with SST pattern changes in the Bay of Bengal (BoB). They also noticed that El Niño connections with the BoB SST contributed to 21.5% of extreme rainfall intensity. Sanap *et al.*[19] also studied the effect of El Niño on NEM by analysing the 1951–2015 data and observed that El Niño years offered favourable conditions for initiation and westward propagation of easterly waves which intensified the rainfall. Srinivas *et al.*[18] used WRF to simulate the Chennai rainfall and studied the effect of planetary boundary layer (PBL) parameterization and grid resolution in the simulations. They found that PBL scheme strongly influenced the prediction of rainfall and out of all selected PBL schemes Mellor–Yamada–Nakanishi–Niino (MYNN) PBL scheme better predicted the event. However, most of these studies are related to the current events and those which occurred in the past. There is no study in the Indian region to predict future changes in rainfall, if such events occur again.

General circulation models (GCMs) have been traditionally used to study the changes in future climate events. However, the low resolution of GCMs which participated in the Coupled Model Inter Comparison Project 5 (CMIP5) hinders their use in the analysis of rainfall events. The PGW method, developed by Schär *et al.*[20], can be used for more accurate modelling of future rainfall events. It allows retaining the daily variation in regional climate by taking realistic initial and boundary conditions. The PGW method has been used to predict future changes of rainfall events in a global warming environment[21–23].

There is a necessity to study the changes in the intensity of rainfall in the future due to the repeated extreme rainfall events. The objective of the present study is to quantitatively analyse the effect of climate change on Chennai 2015-like extreme rainfall events in the far future climate conditions. The future RCP scenario considered in this study is RCP8.5, which is able to capture the possible extremity of climate change.

Model description

The present study uses the advanced research WRF model (WRF–ARW) version 3.7.1, a numerical weather prediction (NWP) model developed by the National Center for Atmospheric Research (NCAR), USA[24]. The WRF–ARW model has been extensively used for simulating heavy rainfall events[25–27], predicting tropical cyclone tracks[28,29] and weather forecasting. Many researchers have successfully simulated the Chennai extreme rainfall event in 2015 using the WRF-ARW model[10,11,17,19]. For this study, we have chosen a two-way, interactive, triple-nested domain with Mercator projection. The higher resolution model (≤3 km) better simulates the exact location of a rainfall event compared to coarse resolution models[17]. In the present study, the innermost domain D03 with 3 km resolution has been considered for further analysis. The first and second domains have a horizontal resolution of 27 km and 9 km respectively. All the domains have 30 vertical levels, with increasing thickness along with the height, and the topmost level is 50 hPa. Figure 1 shows the domain set used in this study and Table 1 provides details of the domain configuration. Table 2 shows the physics parameterization schemes used in the study. The parameterization schemes, except for cumulus (CPS) and microphysics (MPS) were maintained the same in all the simulations. The convective and microphysical schemes represent the cloud and rain process in NWP models[30]. The extreme rainfall events are sensitive to microphysical parameterizations[11].

Data and method

The initial and boundary conditions for current simulations were taken from the National Center for Environmental Prediction Global Forecast System (NCEP GFS) of $0.25° \times 0.25°$ resolution for every 3 h (ref. 31). The SST data were also taken from NCEP GFS of $0.25° \times 0.25°$ resolution[32]. The boundary conditions for the finer domain were received from the output of course domains. Since a two-way nested model has been employed in this study, the output of the finer domain was fed back to the coarser domain at each time step to update the mesh.

The initial and boundary conditions for the future scenarios were obtained by the PGW method that incorporates dynamic downscaling. In the PGW methodology, the climate change signal is calculated by taking the difference between the monthly mean of future climatic condition (2065–2085) and historic condition (1985–2005). The obtained climate change signal, which is temporally constant but spatially varying, is added to current

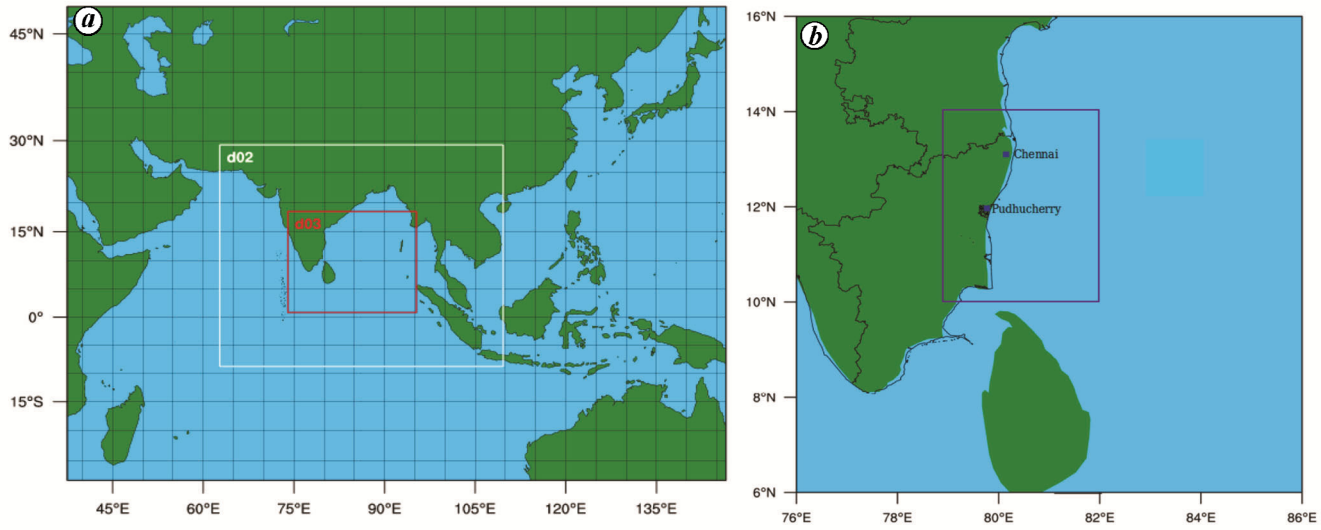

Figure 1. ***a***, Weather Research and Forecasting model domain used in the present study. ***b***, Area used for analysing the results: outer area 6°–16°N and 76°–86°E used for drawing spatial plots; inner box 10°–14°N and 79°–82°E.

Table 1. Model configuration

Number of domains	3
Resolution	D01: dx = dy = 27 km D02: dx = dy = 9 km D03: dx = dy = 3 km
Number of horizontal grid points in X and Y directions	D01: 450 × 350 D02: 580 × 490 D03: 790 × 670
Vertical levels	30
Time step	D01: 120s D02: 40s D03: 13.33s
Central point for D01	13°N, 92°E

Table 2. Physics parameterization schemes used in the study

Longwave radiation	Rapid Radiative Transfer Model (RRTM)
Shortwave radiation	Dudhia scheme
Planetary boundary layer	Yonsei University scheme
Land surface	MM5 similarity
Surface layer	Five-layer thermal diffusion

GFS data to obtain the initial and boundary conditions of future scenario.

Future scenario = Climate change signal

+ GFS current conditions.

In the present study, the NCAR–CESM global bias-corrected data were used for climate change signal calculation[33]. The dataset was obtained from the CCSM4 model output of the CMIP5 archive. The bias correction was done according to Bruyere *et al.*[34], using the European Centre for Medium-Range Weather Forecasts (ECMWF) Interim Reanalysis (ERA-Interim) data.

Previous studies have noted that CCSM4 is a better predictor of Indian summer rainfall and its variability compared to other CMIP5 models[35]. It is to be noted that only the CCSM4 model was used to perturb the current climate and generate forcing data for future climate simulations. The use of ensemble mean based on different climate models could diminish the uncertainty that may arise from using a single model, but it is expected that the general thermodynamic structure of the climate signal would be similar in different models[36].

Figure 2 shows the PGW methodology adopted in this study. Details of the steps involved in WRF simulations are available in the WRF–ARW user guide[37].

The observed precipitation data were taken from tropical rainfall measuring mission (TRMM 3B42-V7) data of 0.25° × 0.25° resolution[38], while wind and moisture data were from ECMWF reanalysis data (ERA5)[39]. In the present study, the TRMM and ERA5 data were used for comparing the current simulation results.

The sensitivities of CPS and MPS parameterization schemes were initially studied. Six combinations of CPS and MPS schemes were chosen based on previous studies in the BoB region[10,29,40]. Phadtare *et al.*[40] used the WRF double moment 5 class (WDM5) microphysics parameterization and Betts–Miller–Janjić (BMJ) cumulus convection scheme for the Chennai rainfall simulations. WRF Single Moment 3 class (WSM3) microphysics scheme and Kain–Fritsch (KF) cumulus convection scheme were used by Boyaj *et al.*[10] for the same event. Kessler (warm rain) microphysics scheme was also seen to perform well in this region. Sandeep *et al.*[29] used the Kessler scheme in the study region for simulating the Vardah cyclone that hit the coast of Chennai in December 2016. Hence, all

combinations of these three microphysics schemes and two cumulus convection schemes were studied. Instead of WSM3, in the present study, WRF Single Moment 6 class (WSM6) which is an advanced version in terms of representation of hydrometeors, was used. The simulations were conducted for all six cases and the results were compared with the observed data. The scheme that gave predictions closer to the observed data was chosen for further studies. Table 3 shows all the six schemes that have been used.

Later, the rainfall event was projected to the far future (2075) for the RCP8.5 scenario using the PGW method. One of the main uncertainties in dynamic downscaling using WRF is that in the initial conditions, which is impossible to remove completely due to observational errors. Ensemble method is one of the methodologies used for reducing uncertainty in the initial conditions[41]. In this method, the model is initialized with different initial conditions and the ensemble mean of these simulations is taken for further analysis. The above-mentioned methodology has been adopted in the present study. The model was initialized with three different initial conditions: (a) 2015–Nov-29_00:00:00UTC, (b) 2015-Nov-29_06:00:00UTC and (c) 2015-Nov-29_12:00:00UTC. The simulations were carried out for both current and future conditions with the best parameterization scheme for these initial conditions. The results were analysed from 30 November 2015 00:00UTC giving a minimum spin-up time of 12 h, so that the simulations had enough time for stabilization[42].

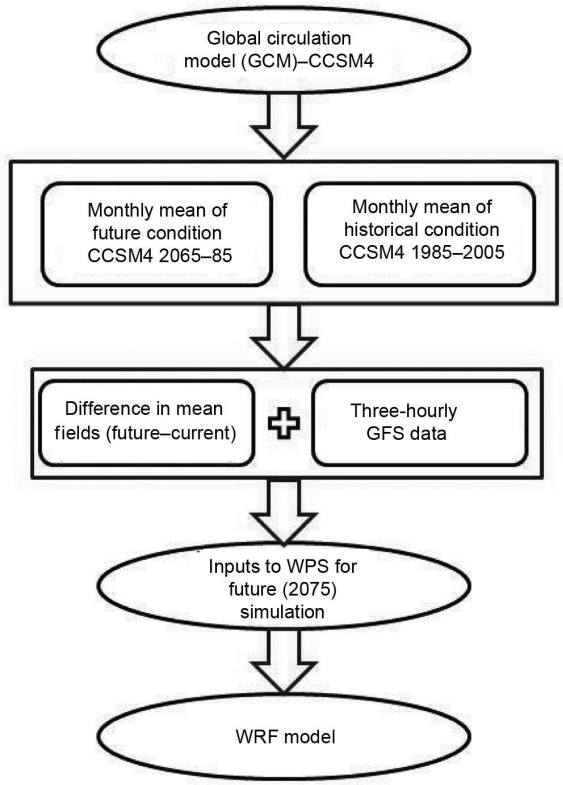

Figure 2. Steps involved in the pseudo global warming method.

Table 3. Sensitivity experiments conducted for the cumulus and microphysics scheme

Case no.	Microphysics scheme	Cumulus scheme
1	WSM6	Kain–Fritsch
2	WDM5	Kain–Fritsch
3	WSM6	Betts–Miller–Janjic
4	WDM5	Betts–Miller–Janjic
5	Kessler	Kain–Fritsch
6	Kessler	Betts–Miller–Janjic

NCAR command language (NCL) version 6.4.0 was used for analysing the outputs from WRF simulations[43]. The TRMM data and ERA 5 data were of $0.25° \times 0.25°$ resolution, while the WRF outputs were of resolution 3 km × 3 km. In order to compare the WRF output with the observed data, the rainfall, moisture convergence and wind values obtained from simulations were regridded to $0.25° \times 0.25°$ using the nearest neighbour method (nearestod).

In the present study, bulk Richardson number (BRN) and energy helicity index (EHI) were used to measure the convective instability in combination with wind shear, and *K*-index was used for measuring the convective instability. BRN was calculated as[44]

$$\text{BRN} = \text{CAPE}/(0.5U^2),$$

where U is the difference between density-weighted mean wind in the layer 0–6 km and mean wind in the layer 0–500 m, and CAPE is taken as the mixed layer convective available potential energy to the lowest 100 hPa. BRN represents the balance between convective instability and wind shear. The high values of BRN refer to more unstable and less sheared environments. However, there is no proper threshold reference to differentiate various storm types. EHI was calculated according to Rasmussen *et al.*[45], and formulated as

$$\text{EHI} = (\text{CAPE}) \times (\text{SRH})/(1.6 \times 10^5),$$

where SRH is the storm-relative helicity to the lowest 3 km and CAPE is the same as used for BRN calculation. Higher EHI values refer to the potential for an intense storm.

The *K*-index was calculated by adding the dry bulb and dew point temperature at 850 hPa and subtracting the sum of the difference of dry bulb and dew point temperatures at 700 hPa and dry bulb temperature at 500 hPa (ref. 46). The equation for calculating the *K*-index is given as

$$K\text{-index} = Td_{850\ \text{hPa}} + T_{850\ \text{hPa}} - T_{500\ \text{hPa}} + (T_{700\ \text{hPa}} - Td_{700\ \text{hPa}}),$$

where T is the dry bulb temperature and Td is the dew point temperature. The K-index value is high when there is abundant moisture in the mid-levels ($Td_{850\ hPa}$), high lapse rate ($T_{850\ hPa} - T_{500\ hPa}$) and low dew point depression ($T_{700\ hPa} - Td_{700\ hPa}$) at 700 hPa. A K-index value greater than 30°C represents favourable conditions for a high storm with likely intense rainfall, and a value more than 40°C indicates high probability of an extreme storm event[46].

Results and discussion

Sensitivity of microphysics and cumulus schemes

The sensitivities of the results to MPS and CPS schemes were first examined to determine the best physics schemes to be used for accurate prediction of an extreme rainfall event like the Chennai event. Simulations for all six combinations of MPS and CPS schemes were performed on the WRF-ARW model in the specified domain for 29 November 2015: 00:00 UTC to 5 December 2015 00:00 UTC, and the results were compared with the observed data.

Since our area of study is the Chennai and Purucherry regions, a small area shown in Figure 1 was considered for obtaining the daily average rainfall. Figure 3 shows the area-averaged rainfall in the specified region 10°–14°N and 79°–82°E from 30 November 2015 to 4 December 2015 for all the cases compared with the TRMM data. The TRMM data show peak rainfall on 1 December 2015. According to the TRMM data, 140 mm rainfall was recorded in the specified region on 1 December 2015. Only case 5 (Kessler and KF) showed peak rainfall on 1 December 2015, even though it was under-predicting the peak rainfall. During other days too, case 5 was seen to capture the exact trend of TRMM data. Cases 1–3 showed two peaks in the rainfall plot, on 30 November and 2 December 2015, and low rainfall on 1 December 2015 compared to the TRMM data. Case 6 showed an increasing trend of rainfall from 30 November to 2 December 2015. Figure 4 shows the spatial comparison plot of 1 December 2015 rainfall for all the six cases with the TRMM data. The TRMM data showed high precipitation (>200 mm) in the region 79°–81°E and 11°–14°N, and only case 5 showed high rainfall in this region. Similar to the daily-averaged rainfall plot, all other cases showed lower amounts of rainfall in the region and the peak rainfall region did not coincide with Chennai and Puducherry.

Figure 5 shows the moisture convergence on 1 December 2015 at 1000 hPa for all the cases compared to the ERA-5 data. In all the six cases, moisture convergence showed good agreement with the ERA-5 data, both quantitatively and spatially. The high moisture convergence in the coastal areas in the region 10°–15°N in the ERA-5 data was precisely reproduced by all the six cases. Wind streamlines at 850 hPa were plotted for all the six cases and compared with ERA-5 data (Figure 6). The ERA-5 data showed circulation in the region 8°E and 80°N. Cases 3, 5 and 6 reproduced a circulation on 1 December 2015. However, spatial matching with the ERA-5 data was not good.

From the comparison of all six cases with the observed data, it can be concluded that a warm rain microphysics scheme (Kessler) in combination with KF cumulus convection scheme (case 5) is able to capture the trend of rainfall pattern reasonably well and is the best available model. The moisture convergence and wind streamlines too agree well with the observed data for case 5. In consideration of the above reasons, case 5 was chosen for further studies.

The extreme rainfall event was involved with complex moist convection processes, which are better represented in the KF scheme compared to the BMJ scheme. The moist processes below cloud base level were not included in the BMJ scheme[47]. The strong lower-level moisture dynamics associated with mid-level cyclonic circulation was the critical factor in this event[18]. The low-level moisture processes are well parameterized in the Kessler warm rain microphysics scheme. The Kessler scheme is involved with only three hydrometeors like water vapour, cloud and rain. The involvement of other hydrometeors such as ice, snow and graupel in WSM6 and WDM5 (ice and snow) may have resulted in the under-prediction of heavy surface rainfall of this particular event, which is highly influenced by low-level moisture convergence.

The 21-year climatological mean difference

The precipitation is positively correlated with temperature and moisture content in the atmosphere. Hence it is

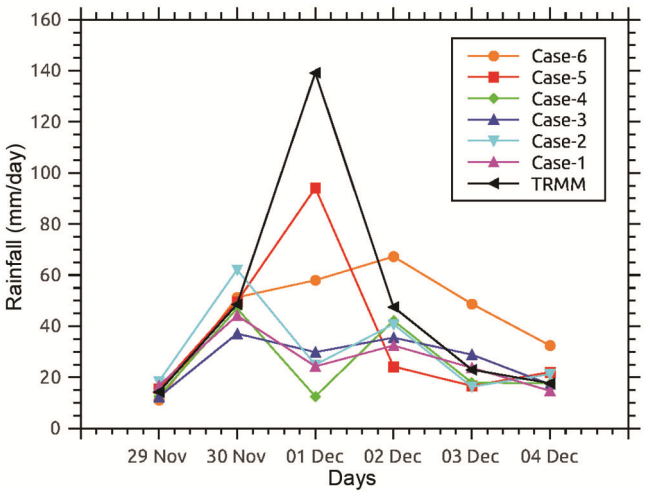

Figure 3. Time series of area-averaged rainfall (10°–14°N, 79°–82°E) for all the six cases compared with tropical rainfall measuring mission (TRMM) observed data.

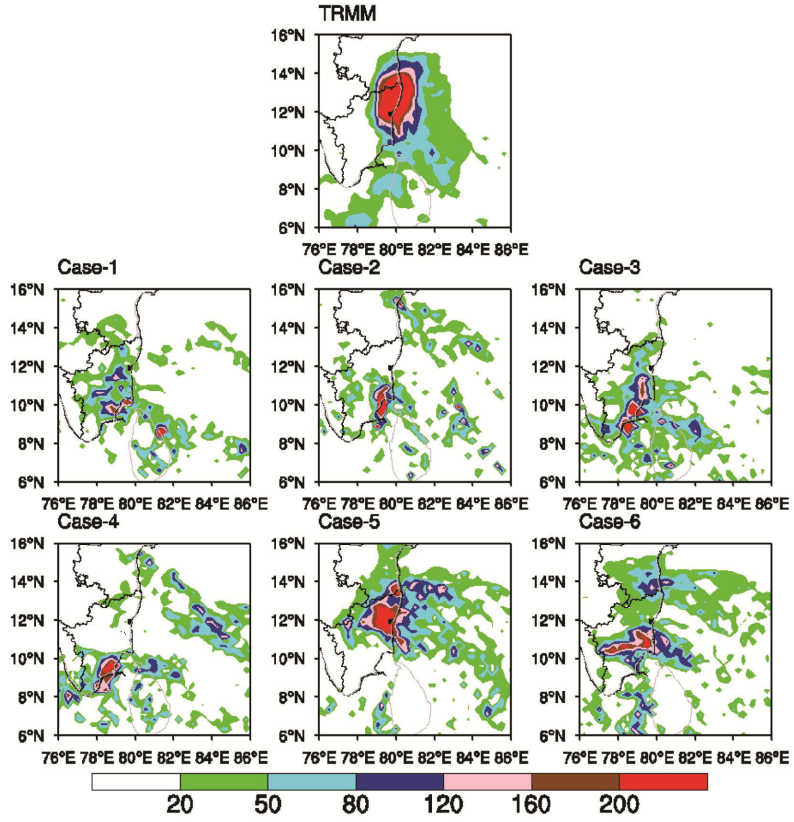

Figure 4. Spatial plot of 1 December 2015 rainfall (mm) for all six considered cases compared with TRMM observed data.

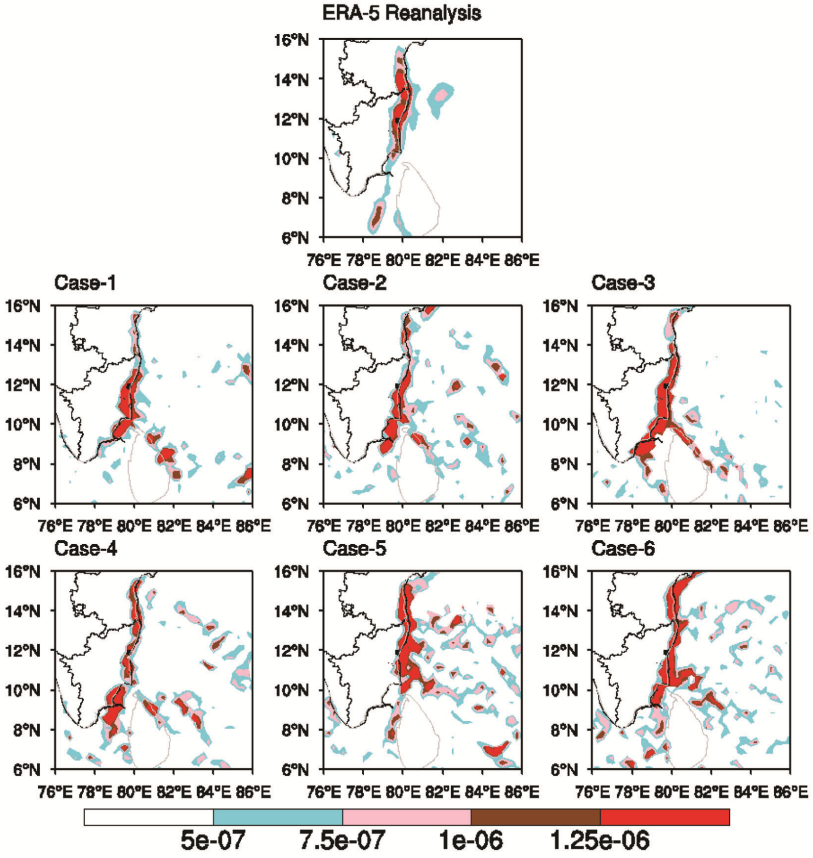

Figure 5. Moisture convergence (kg/kg-sec) at 1000 hPa on 1 December 2015 for all six cases compared with ERA5 Reanalysis data.

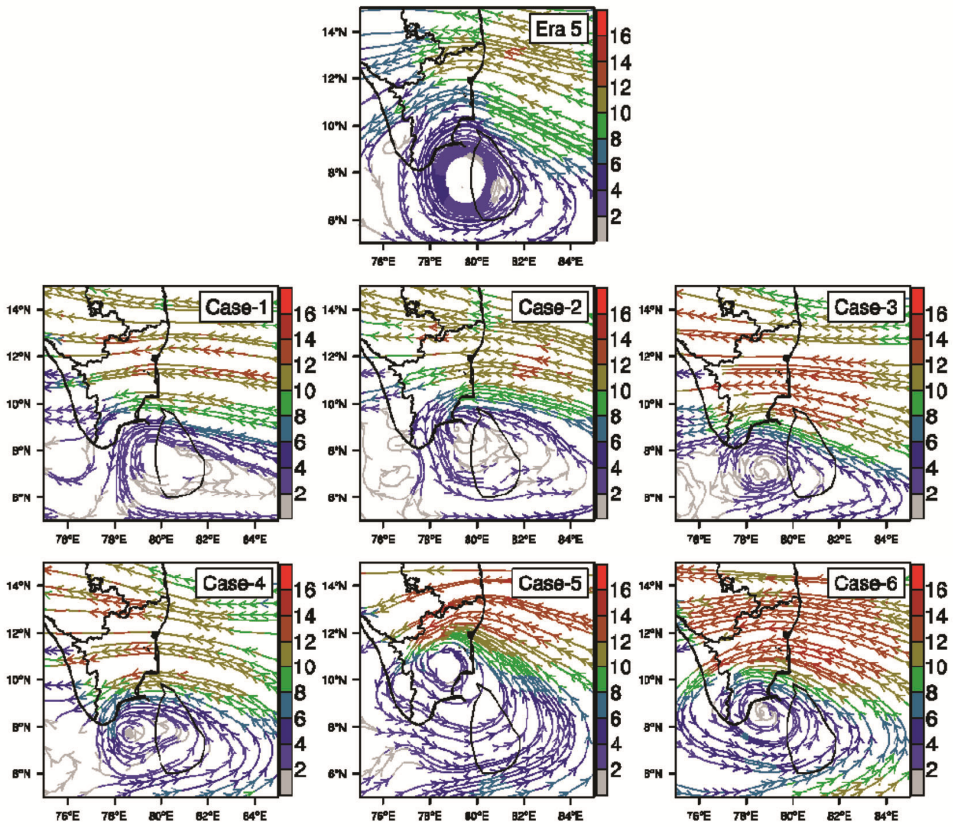

Figure 6. Streamline plot with wind magnitude (m/s) at 850 hPa on 1 December 2015 for all six cases compared with ERA5 Reanalysis data.

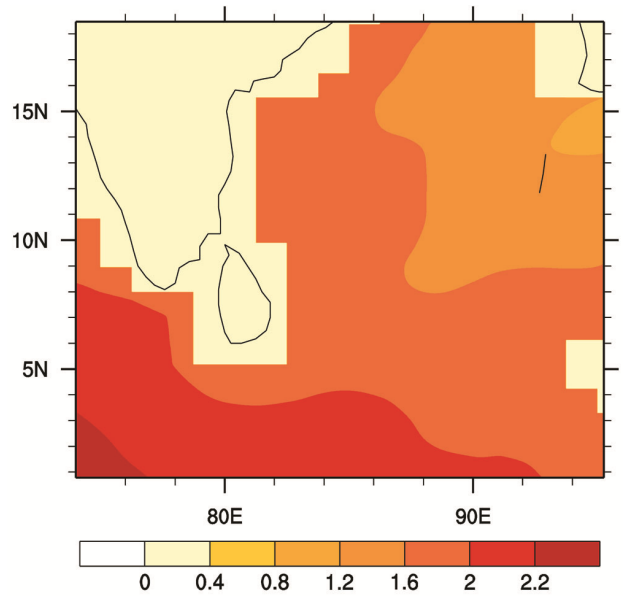

Figure 7. The 21-year mean difference (future – historical) of sea surface temperature (K) for December in representative concentration pathway the (RCP) 8.5 scenario.

imperative to study the change in SST and moisture content with climate change. Figure 7 shows the 21-year climatological mean difference of SST between far future RCP8.5 scenario and historic period in December. There was a noticeable increase in SST in future conditions and in some regions, it was more than 2°C. The increase in most parts of the BoB region was more than 1.6°C. Figure 8 shows the increase of surface temperature over the Indian region in December. Over the east coast of India, the increase was more than 2°C. Figure 9 shows the 21-year climatological mean difference of water vapour mixing ratio (Q) between the far future and present condition. A significant increase from 1 to 3 g/kg over the BoB region was observed. These conditions are favourable for an increase in precipitation in future climate conditions.

Atmospheric instability also plays a major role in the amount of precipitation. In this study, changes in the K-index value in future have been estimated. Figure 10 shows a 1.75°C increase in the K-index value in future conditions over most of the domain. This significant increase in the K-index represents a more unstable atmosphere in the future warming climate.

Atmospheric conditions

The atmospheric instabilities, moisture content, temperature and wind play a crucial role in the precipitation amount and intensity. In the present study, the K-index,

BRN number and EHI were used to represent atmospheric instability. Figure 11 shows the daily averaged *K*-index for current and future ensembles averaged over the domain 10°–14°N and 79°–82°E. The *K*-index value was more than 30°C for both future and current ensembles throughout the simulations. The highest *K*-index value in the current and future simulations was 36.4°C and 37.2°C respectively. The maximum *K*-index value in both the current and future simulations occurred on 1 December. Except on 30 November, the *K*-index values increased in

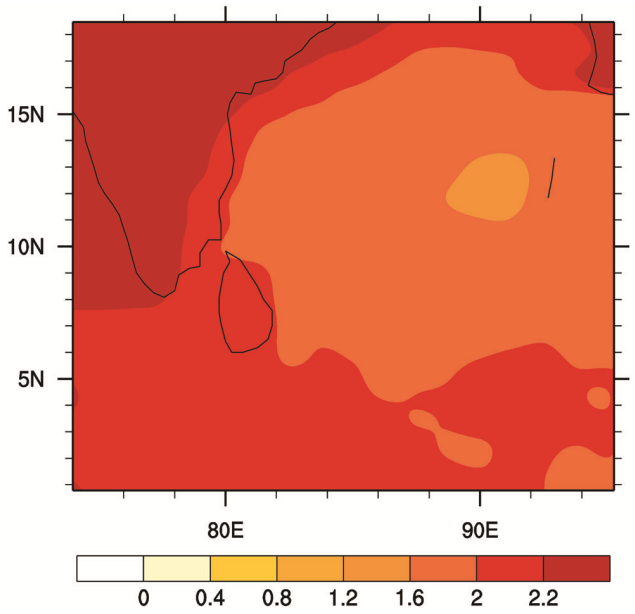

Figure 8. The 21-year mean difference (future – historical) of surface temperature (K) for December in the RCP 8.5 scenario.

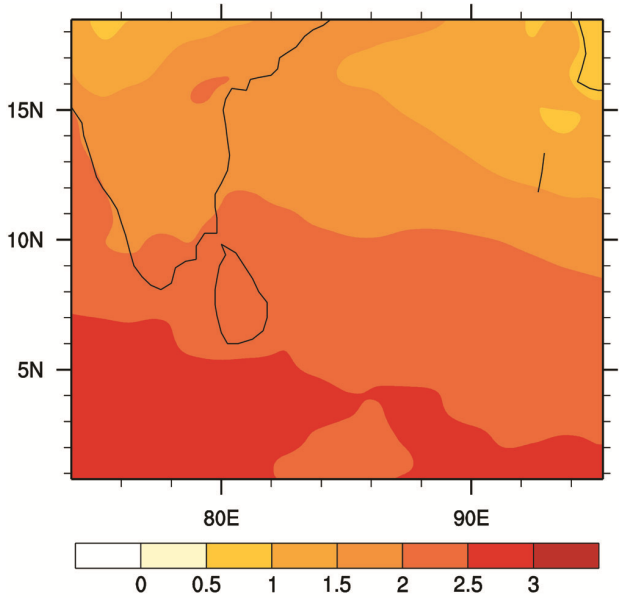

Figure 9. The 21-year mean difference (future – historical) of water vapour mixing ratio (g/kg) for December in the RCP 8.5 scenario.

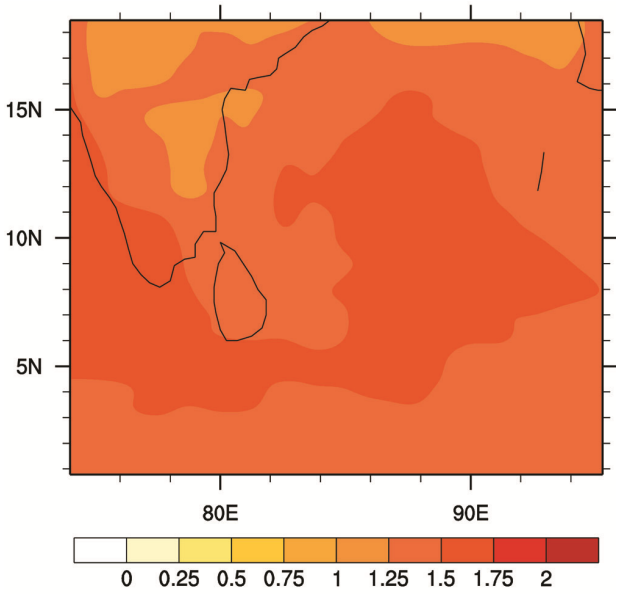

Figure 10. The 21-year mean difference (future – historical) of *K*-index (°C) value for December in the RCP 8.5 scenario.

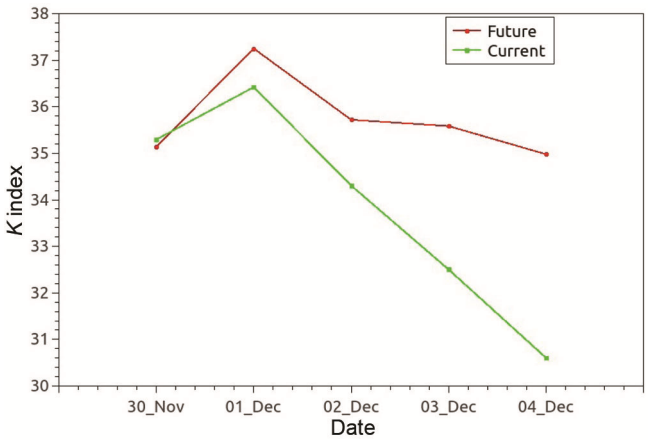

Figure 11. Time series of area-averaged *K*-index value (10°–14°N, 79°–82°E) for future and current ensemble mean.

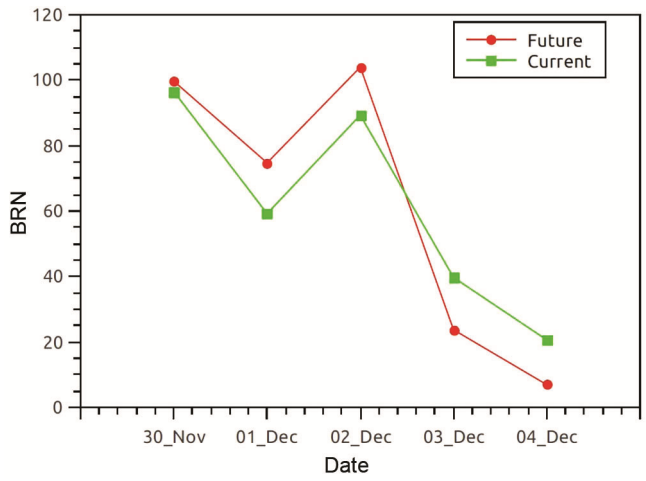

Figure 12. Daily averaged bulk Richardson number for current and future ensembles averaged over the domain 10°–14°N and 79°–82°E.

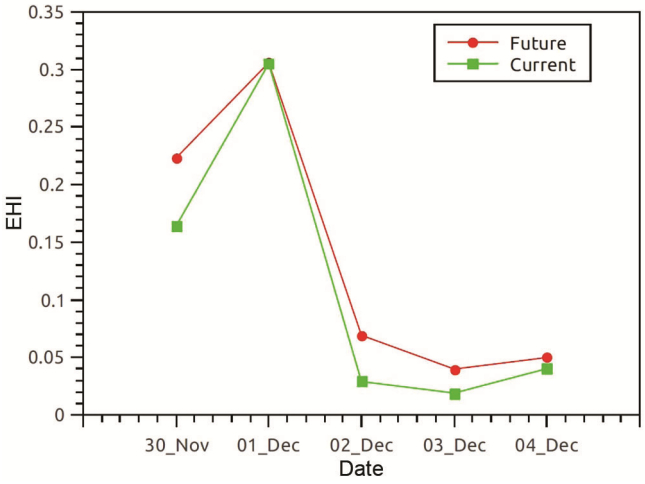

Figure 13. Daily averaged energy helicity index for current and future ensembles averaged over the domain 10°–14°N and 79°–82°E.

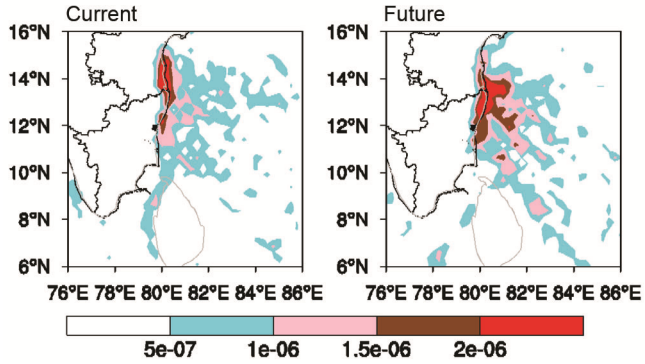

Figure 14. Moisture convergence (kg/kg-sec) at 1000 hPa of 1 December for current and future ensemble means.

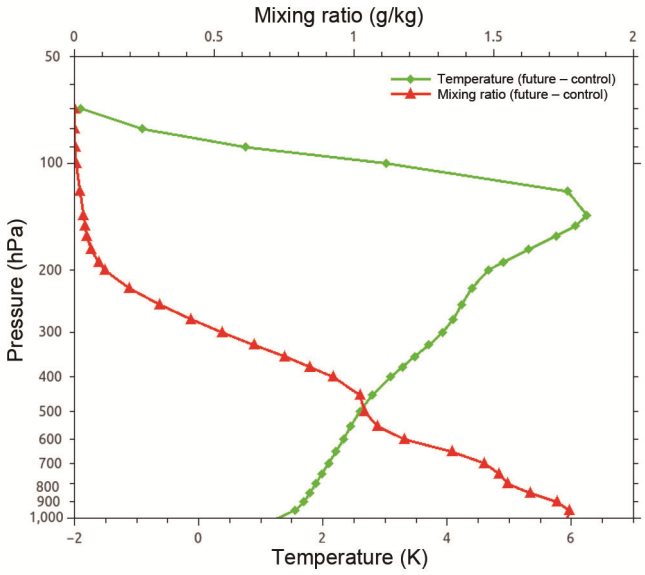

Figure 15. Change in vertical profile of temperature and mixing ratio (future – current) averaged over the domain 10°–14°N and 79°–82°E on 1 December.

the future compared to the current. The increase was about 2.27%, 4.11%, 9.47% and 14.9% on 1, 2, 3 and 4 December respectively.

Figure 12 shows the daily averaged BRN for current and future ensembles averaged over the domain 10°–14°N and 79°–82°E. A significant increase in the BRN values was observed in the future compared to current values on 1 and 2 December respectively. The increased BRN values represent a more unstable and less sheared environment, which could be favourable for high precipitation events. However, there was a decrease in the BRN values on 3 and 4 December in the future compared to the current. This may be associated with an increase in wind shear.

Figure 13 shows the daily averaged EHI for current and future ensembles averaged over the domain 10°–14°N and 79°–82°E. The maximum EHI value in both the current and future simulations occurred on 1 December. The EHI values increased in the future compared to the current for all the five days. This suggests that instabilities in the atmosphere are likely to increase in the future.

Figure 14 shows the moisture convergence at 1000 hPa for current and future ensembles for 1 December. Similar to the *K*-index plot, an increased moisture convergence was seen in future compared to the current scenario on 1 December. In both the future and current scenario ensembles, moisture convergence was higher than 1×10^{-6} kg/kg s in the coastal area from 11°N to 15°N. Additionally, the area having moisture convergence value higher than 2×10^{-6} kg/kg s was found to increase in future simulations in the coastal regions as well as over the sea. Increased moisture flux convergence values usually lead to an increase in precipitation[48].

The vertical distribution of temperature and water vapour mixing ratio was examined over the Chennai region. Figure 15 shows the change in vertical distribution of temperature and mixing ratio for 1 December over the domain 10°–14°N and 79°–82°E. Between 400 hPa and 120 hPa, the warming was more than 3°C, which is quite significant. The temperature in future was seen to increase throughout the troposphere and a reversal in the trend was seen above the troposphere. The water vapour content in the atmosphere increased in the troposphere for future climate conditions and the increase was maximum on the surface, which is equal to 1.76 g/kg. These results are consistent with a previous study by Mittal *et al.*[49], who stated that the warm and moist tropospheric conditions lead to an increase in atmospheric instabilities.

Figure 16 shows the streamline plot of winds at 850 hPa level for current and future ensembles. No significant variation in the wind in terms of magnitude and direction was observed in the Chennai region. However, the low-pressure region had slightly shifted towards the south in future compared to current simulations.

The changes in SST, surface temperature and water vapour mixing ratio are some of the reasons for changing

the atmospheric thermodynamics explained here. These changes are favourable for precipitation and hence in future climate conditions, the probability of heavy rainfall increases.

Future changes in Chennai rainfall

Figure 17 shows area-averaged rainfall over the region 10°–14°N and 79°–82°E from 30 November 2015 to 4 December 2015 for the current and future ensemble means. The rainfall pattern for the future showed the same trend as observed in the current condition. The total cumulative rainfall obtained for the five days (30 November 00:00UTC to 5 December 00:00 UTC) was found to increase by 33.32% for future conditions. The peak rainfall was on 1 December 2015 in both future and current conditions, in the future peak rainfall was seen to increase by 17.4% compared to the current rainfall. On 2, 3 and 4 December 2015, the increase in rainfall was 183.5%, 233.9% and 70.8% respectively. The precipitation pattern agreed well with the *K*-index and moisture convergence changes. Hence, it is evident that the increased amount of rainfall in the future could be due to atmospheric instability, availability of high moisture and warm SST. The increase in the maximum and total rainfall in the future scenario points to the likelihood of dangerous and prolonged flood situation in this region. Figure 18 shows the spatial plot of total precipitation for future and current ensembles for 1, 2 and 3 December 2015. The coastal area receiving more than 200 mm (red colour) of rainfall increased in the future, even though the total area (including green colour) had decreased. Hence in future, there could be a likely increase in the area receiving high-intensity rainfall.

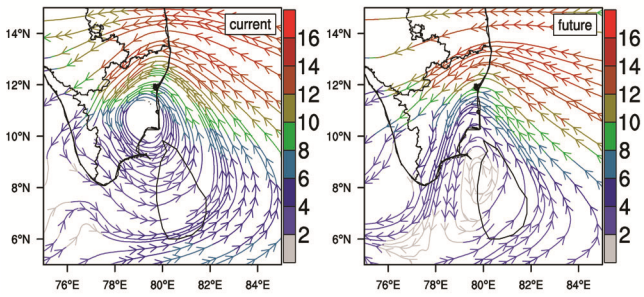

Figure 16. Streamline plot with wind magnitude (m/s) at 850 hPa of 1 December for current and future ensemble means.

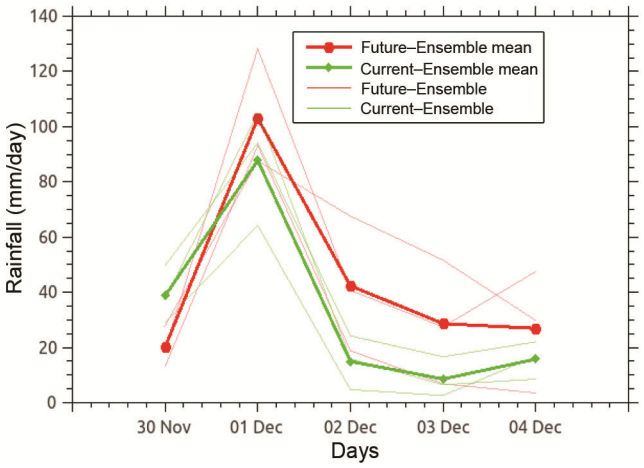

Figure 17. Time series of area averaged rainfall (10°–14°N, 79°–82°E) of current and future runs (dark line: ensemble; light lines: simulations for three different initial conditions).

Conclusion

The main objective of this study was to quantitatively evaluate the effect of climate change on the characteristics of a heavy-rainfall event that occurred in the coastal city of Chennai in December 2015. The high-resolution WRF model was used for the simulations. Initially, the sensitivity of CPC and MPS schemes was studied for six different cases on accurately simulating the 2015 Chennai rainfall. The results of warm rain microphysics (Kessler) scheme and KF cumulus scheme were seen to agree well with the observed data. These schemes were able to capture the observed rainfall trend, even though they underpredicted the highest rainfall. These physics schemes were then used for studying the changes in future rainfall events.

A comparison of future and current rainfall events was carried out later. Simulations were done for both future and current conditions. Ensemble method was used to reduce the uncertainty associated with the initial conditions. PGW dynamic downscaling method was adopted for representing the simulations for future climate conditions and projections were done for the far future (2075) RCP8.5 scenario. CCSM4 GCM data were used for obtaining the climate change signal using the PGW method. The climate change signal thus obtained was added to the initial and boundary conditions of the current scenario, which gave the initial and boundary conditions of the future climate.

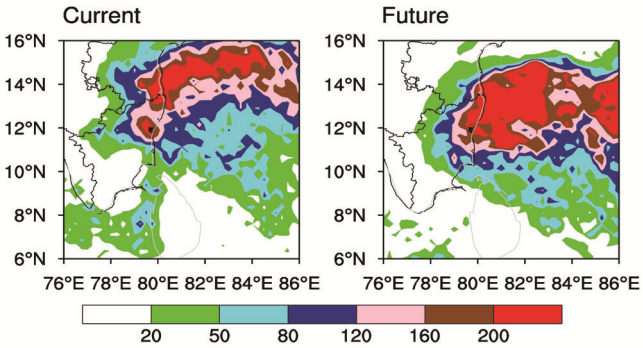

Figure 18. Spatial plot of total precipitation (mm) for future and current ensembles for 1, 2 and 3 December.

The results show that in the future scenario, SST, surface temperature and moisture content in the atmosphere increase in the BoB region. The increase in these quantities can lead to an increase in atmospheric instability and moisture convergence. In the present study, BRN and EHI were used to measure the convective instability in combination with wind shear, and *K*-index was used for measuring the convective instability. All these parameters showed an increase in atmospheric instability compared to the current simulation. Similarly, moisture convergence, vertical value of temperature and mixing ratio showed an increase on 1 December 2015 in future climate conditions. The increase in these quantities is favourable for heavy precipitation. So the projection shows increase in precipitation on 1 December and consecutive days. The total increase in precipitation for five days, from 30 November to 4 December 2015 was 33.32%. On 1 December 2015, which is the peak rainfall day, the increase in precipitation in future over the Chennai region was found to be more than 17% and for the next consecutive days, the increment was 183.5%, 233.9% and 70.8% respectively. The geographical extent of the region receiving more than 200 mm of rainfall for three days was seen to increase in future climatic conditions. The size and intensity of heavy rainfall events can increase significantly in the far-future high-emission scenario climate conditions. If a similar event occurs in the future, the flood conditions are likely to continue for more days compared to the current event, thereby signifying increased risks; this would require better preparations to face the disaster. This study considers only one event, and thus the results are suggestive. Furthermore, several cases during different seasons (pre-monsoon and post-monsoon) need to be studied to arrive at a better conclusion for the responses of extreme rainfall events to climate change.

1. Eckstein, D., Hutfils, M. and Winges, M., Global climate risk index 2019. Germanwatch; https://germanwatch.org/en/16046 (accessed on 23 August 2019).
2. Wasson, R. J. *et al.*, Riverine flood hazard: disaster risk reduction in India. *Proc. Indian Natl. Sci. Acad*., 2018, **99**, 65–76.
3. Mukherjee, S., Aadhar, S., Stone, D. and Mishra, V., Increase in extreme precipitation events under anthropogenic warming in India. *Weather Climate Extrem*., 2018, **20**, 45–53.
4. Goswami, B. N., Venugopal, V., Sangupta, D., Madhusoodanan, M. S. and Xavier, P. K., Increasing trend of extreme rain events over India in a warming environment. *Science*, 2006, **314**, 1442–1445.
5. Mishra, A. K., Quantifying the impact of global warming on precipitation patterns in India. *Meteorol. Appl.*, 2019, **26**, 153–160.
6. Prakash, S., Mahesh, C., Sathiyamoorthy, V. and Gairola, R. M., Increasing trend of northeast monsoon rainfall over the equatorial Indian Ocean and peninsular India. *Theor. Appl. Climatol*., 2013, **112**, 185–191.
7. Mishra, A. K. and Nagaraju, V., Space-based monitoring of severe flooding of a southern state in India during south-west monsoon season of 2018. *Nat. Hazards*, 2019, **97**, 949–953.
8. Mishra, V. and Shah, H. L., Hydroclimatological perspective of the Kerala flood of 2018. *J. Geol. Soc. India*, 2018, **92**, 645–650.
9. Kerala rains: 1038 villages declared flood-hit, *The Hindu*, 25 August 2019, p. 2.
10. Boyaj, A., Ashok, K., Ghosh, S., Devanand, A. and Dandu, G., The Chennai extreme rainfall event in 2015: the Bay of Bengal connection. *Climate Dyn.*, 2018, **50**, 2867–2879.
11. Reshmi Mohan, P., Srinivas, C. V., Yesubabu, V., Baskaran, R. and Venkatraman, B., Simulation of a heavy rainfall event over Chennai in southeast India using WRF: sensitivity to microphysics parameterization. *Atmos. Res*., 2018, **210**, 83–99.
12. Intergovernmental Panel on Climate Change, *Climate Change 2014: Synthesis Report. Contribution of Working Groups I, II and III to the Fifth Assessment Report of the Intergovernmental Panel on Climate Change* (eds Pachauri, R. K. and Meyer, L. A.), IPCC, Geneva, Switzerland, 2015.
13. Willett, K. M., Gillett, N. P., Jones, P. D. and Thorne, P. W., Attribution of observed surface humidity changes to human influence. *Nature*, 2007, **449**, 710–712.
14. Min, S. K., Zhang, X., Zwiers, F. W. and Hegerl, G. C., Human contribution to more intense precipitation extremes. *Nature*, 2011, **470**, 378–381.
15. Prein, A. F., Rasmussen, R. M., Ikeda, K., Liu, C., Clark, M. P. and Holland, G. J., The future intensification of hourly precipitation extremes. *Nature Climate Change*, 2017, **7**, 48–52.
16. Trenberth, K. E., Dai, A., Rasmussen, R. M. and Parsons, D. B., The changing character of precipitation. *Bull. Am. Meteorol. Soc.*, 2003, **84**, 1205–1217 + 1167.
17. Singh, K. S., Bonthu, S., Purvaja, R., Robin, R. S., Kannan, B. A. M. and Ramesh, R., Prediction of heavy rainfall over Chennai Metropolitan City, Tamil Nadu, India: impact of microphysical parameterization schemes. *Atmos. Res*., 2018, **202**, 219–234.
18. Srinivas, C. V., Yesubabu, V., Prasad, D. H., Prasad, K. H., Greeshma, M. M., Baskaran, R. and Venkatraman, B., Simulation of an extreme heavy rainfall event over Chennai, India using WRF: sensitivity to grid resolution and boundary layer physics. *Atmos. Res.*, 2018, **210**, 66–82.
19. Sanap, S. D., Priya, P., Sawaisarje, G. K. and Hosalikar, K. S., Heavy rainfall events over southeast peninsular India during northeast monsoon: role of El Niño and easterly wave activity. *Int. J. Climatol.*, 2019, **39**, 1954–1968.
20. Schär, C., Frei, C., Lüthi, D. and Davies, H. C., Surrogate climate-change scenarios for regional climate models. *Geophys. Res. Lett.*, 1996, **23**, 669–672.
21. Taniguchi, K. and Sho, K., Application of the pseudo global warming dynamic downscaling method to the Tokai heavy rain in 2000. *J. Meteorol. Soc. Jpn.*, 2015, **93**, 551–570.
22. Scalzitti, J., Strong, C. and Kochanski, A., Climate change impact on the roles of temperature and precipitation in western US snowpack variability. *Geophys. Res. Lett.*, 2016, **43**, 5361–5369.
23. Expósito, F. J., González, A., Pérez, J. C., Díaz, J. P. and Taima, D., High-resolution future projections of temperature and precipitation in the Canary Islands. *J. Climate*, 2015, **28**, 7846–7856.
24. Skamarock, W. C. *et al.*, A Description of the Advanced Research WRF Version 3, NCAR Technical Note, NCAR/TN-468+STR, 2008.
25. Kedia, S., Vellore, R. K., Islam, S. and Kaginalkar, A., A study of Himalayan extreme rainfall events using WRF-Chem. *Meteorol. Atmos. Phys.*, 2019, **131**, 1133–1143.
26. Hong, S. Y. and Lee, J. W., Assessment of the WRF model in reproducing a flash-flood heavy rainfall event over Korea. *Atmos. Res*., 2009, **93**, 818–831.
27. Mugume, I. *et al.*, Assessing the performance of WRF model in simulating rainfall over western Uganda. *J. Climatol. Weather Forecast.*, 2017, **5**, 1–9.
28. Mohanty, U. C., Osuri, K. K., Routray, A., Mohapatra, M. and Pattanayak, S., Simulation of Bay of Bengal tropical cyclones with

WRF model: impact of initial and boundary conditions. *Mar. Geod*., 2010, **33**, 294–314.
29. Sandeep, C. P. R., Krishnamoorthy, C. and Balaji, C., Impact of cloud parameterization schemes on the simulation of cyclone Vardah using the WRF model. *Curr. Sci.*, 2018, **115**, 1143–1153.
30. Powers, J. G. *et al.*, The Weather Research and Forecasting model: overview, system efforts, and future directions. *Bull. Am. Meteorol. Soc.*, 2017, **98**, 1717–1737.
31. National Centers for Environmental Prediction/National Weather Service/NOAA/US. Department of Commerce. NCEP GFS 0.25 degree global forecast grids historical archive. Research Data Archive at the National Center for Atmospheric Research, Computational and Information Systems Laboratory, 2015 (updated daily); https://doi.org/10.5065/D65D8PWK (accessed on 10 June 2019).
32. Reynolds, R. W., Smith, T. M., Liu, C., Chelton, D. B., Casey, K. S. and Schlax, M. G., Daily high-resolution-blended analyses for sea surface temperature. *J. Climate*, 2007, **20**, 5473–5496.
33. Monaghan, A. J., Steinhoff, D. F., Bruyere, C. L. and Yates, D., NCAR CESM global bias-corrected CMIP5 output to support WRF/MPAS research. Research Data Archive at the National Center for Atmospheric Research, Computational and Information Systems Laboratory, 2014; https://doi.org/10.5065/D6DJ5CN4 (accessed on 10 June 2019).
34. Bruyère, C. L., Done, J. M., Holland, G. J. and Fredrick, S., Bias corrections of global models for regional climate simulations of high-impact weather. *Climate Dyn*., 2013, **43**, 1847–1856.
35. Jayasankar, C. B., Surendran, S. and Rajendran, K., Robust signals of future projections of Indian summer monsoon rainfall by IPCC AR5 climate models: role of seasonal cycle and interannual variability. *Geophys. Res. Lett.*, 2015, **42**, 3513–3520.
36. Rasmussen, R. *et al.*, High-resolution coupled climate runoff simulations of seasonal snowfall over Colorado: a process study of current and warmer climate. *J. Climate*, 2011, **24**, 3015–3048.
37. Mesoscale and Microscale Meteorology Division, and National Center for Atmospheric Research. *ARW Version 3 Modelling System User's Guide*, January 2016; In Book http://www2.mmm.ucar.edu/wrf/users/docs/user_guide_V3.6/contents.html.
38. Huffman, G., TRMM (TMPA-RT) near real-time precipitation L3 3 hour 0.25° × 0.25° V7, Goddard Earth Sciences Data and Information Services Center (GES DISC), Greenbelt, MD, USA, 2016; https://disc.gsfc.nasa.gov/datacollection/TRMM_3B42RT_7.html (accessed on 10 June 2019).
39. Copernicus Climate Change Service (C3S): ERA5: Fifth generation of ECMWF atmospheric reanalyses of the global climate. Copernicus Climate Change Service Climate Data Store (CDS), 2017; https://cds.climate.copernicus.eu/cdsapp#!/home (accessed on 15 June 2019).
40. Phadtare, J., Role of Eastern Ghats orography and cold pool in an extreme rainfall event over Chennai on 1 December 2015. *Mon. Weather Rev.*, 2018, **146**, 943–965.
41. Zhao, J., Guo, Z. H., Su, Z. Y., Zhao, Z. Y., Xiao, X. and Liu, F., An improved multi-step forecasting model based on WRF ensembles and creative fuzzy systems for wind speed. *Appl. Energ*., 2016, **162**, 808–826.
42. Ulmer, F.-G. and Balss, U., Spin-up time research on the Weather Research and Forecasting model for atmospheric delay mitigations of electromagnetic waves. *J. Appl. Remote Sensing*, 2016, **10**, 016027.
43. The NCAR Command Language (Version 6.4.0), UCAR/NCAR/CISL/TDD, Boulder, Colorado, USA, 2017; http://dx.doi.org/10.5065/D6WD3XH5.
44. Stensrud, D. J., Cortinas, J. V. and Brooks, H. E., Discriminating between tornadic and non tornadic thunderstorms using mesoscale model output. *Weather Forecast*., 1997, **12**, 613–632.
45. Rasmussen, E. N., Refined supercell and tornado forecast parameters. *Weather Forecast*., 2003, **18**, 530–535.
46. da Silva, F. P., Rotunno Filho, O. C., Sampaio, R. J., Dragaud, I. C., de Araújo, A. A., da Silva, M. G. and Pires, G. D., Evaluation of atmospheric thermodynamics and dynamics during heavy-rainfall and no-rainfall events in the metropolitan area of Rio de Janeiro, Brazil. *Meteorol. Atmos. Phys*., 2019, **131**, 299–311.
47. Kanase, R. D. and Salvekar, P. S., Effect of physical parameterization schemes on track and intensity of cyclone LAILA using WRF model. *Asia-Pac. J. Atmos. Sci.*, 2015, **51**, 205–227.
48. Wei, J., Su, H. and Yang, Z. L., Impact of moisture flux convergence and soil moisture on precipitation: a case study for the southern United States with implications for the globe. *Climate Dyn.*, 2016, **46**, 467–481.
49. Mittal, R., Tewari, M., Radhakrishnan, C., Ray, P., Singh, T. and Nickerson, A. K., Response of tropical cyclone Phailin (2013) in the Bay of Bengal to climate perturbations. *Climate Dyn*., 2019, **53**, 2013–2030.

ACKNOWLEDGEMENTS. This research has been carried out as part of the project 'Climate change impacts on coastal infrastructure and the adaptation strategies' (Project No: CIE1819265DSTXSACI) funded by the Department of Science and Technology, Government of India under the SPLICE-climate change programme.

Received 22 November 2019; revised accepted 2 March 2020

doi: 10.18520/cs/v118/i12/1968-1979